Technical Report / Research

Property of Wear and Rolling Contact Fatigue Damage in High-hardness Pearlitic Steels

Masaharu UEDA* Takeshi YAMAMOTO
Kyohei SONOYAMA

Abstract

On overseas heavy haul railways, the environment in which the rails are used has become severe due to the increased wheel load associated with higher cargo loads. At the rail heads that come into contact with the wheels, wear and rolling contact fatigue damage has become evident. In response to these issues, many studies are being conducted on the wear resistance and rolling contact fatigue damage resistance of rail steel, but there are few results that comprehensively evaluate the effects of the hardness and carbon content of rail steel. Therefore, we evaluated the wear and rolling contact fatigue damage properties of high-hardness pearlite steel using a two-cylinder testing machine that simulates a heavy haul railway. Furthermore, the hardness and plastic flow of the rolling surface were investigated, and the governing factors of wear and the mechanism of fatigue damage generation were discussed based on tribology and fracture mechanics approaches.

1. Introduction

Overseas freight railways, vital for transporting natural resources such as iron ore and grains, are actively increasing cargo payloads to boost transportation efficiency. However, this strategic move has significantly increased the wheel load of freight cars, creating a more severe operating environment. The rail heads, which come into contact with the wheels, are now facing a critical issue of escalating wear and rolling contact fatigue (RCF) damage due to the amplified contact surface pressure and tangential force (friction force).[1)]

Figure 1 shows examples of wear and rolling contact fatigue damage that occurred in freight railways. The contact surface between the rail and the wheel is subjected to the contact pressure due to the rolling of the wheel and the tangential force in the opposite direction to the rolling direction. In particular, slip occurs in the gauge corner (G.C.) of the rail due to the contact between the gauge corner and the wheel flange, and a large tangential force acts on the gauge corner. As a result, wear accelerates on the rolling contact surface, and a large plastic flow occurs beneath the rolling contact surface. Furthermore, cracks are generated in the plastic flow region due to repeated contact, and the propagation of the cracks causes rolling contact fatigue damage accompanied by peeling, known as spalling.[2–5)]

Regarding these issues, various studies have been conducted on rail wear and rolling contact fatigue damage. The effects of the hardness and carbon content of pearlitic steels with high carbon content on the wear have been discussed. Increasing the hardness of pearlitic steel has been reported to be effective in improving the wear resistance of rails.[6–8)] Furthermore, increasing the carbon content of pearlitic steel has been reported to be effective in improving the wear resistance of rails.[9)] Also, the correlation between rolling contact fatigue damage and the hardness of pearlitic steel has been discussed for some time. Increasing the hardness of the pearlitic steel has been reported to be effective in suppressing the plastic flow of the rolling contact surface.[10–12)] Moreover, the correlation with the carbon content has been discussed. Increasing the carbon content of the pearlitic steel is reported to be effective in suppressing the plastic flow and crack propagation and improving the rolling contact fatigue damage resistance.[13)] However, there have been few studies that comprehensively evaluated the effects of the hardness and carbon content of the pearlitic steel with high hardness and high carbon content on the wear and rolling contact fatigue damage properties and discussed the mechanisms involved.

This report aims to clarify the effect of the initial hardness and

* Dr. Eng., General Manager, Rail & Shape Div., Kyushu Works
1-1 Tobihata-cho, Tobata-ku, Kitakyushu City, Fukuoka Pref. 804-8501

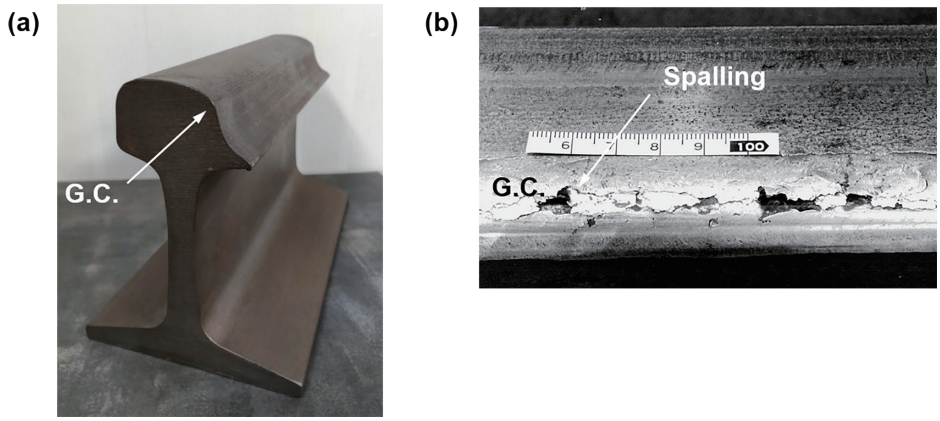

Fig. 1 Examples of wear and rolling contact fatigue damage on overseas heavy haul railways: (a) Worn rail, (b) Rolling contact fatigue damaged rail

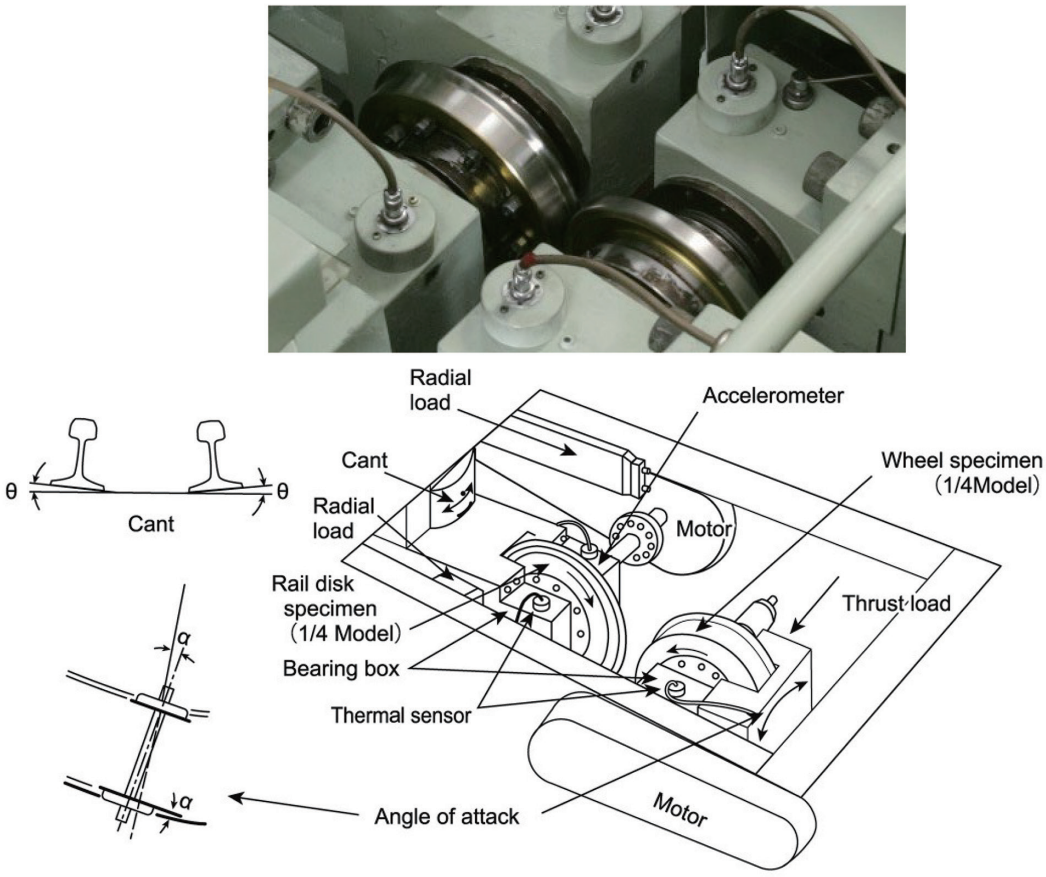

Fig. 2 Appearance and schematic outline of a two-disk-type testing machine

carbon content of pearlitic steel with high hardness and high carbon content on the wear resistance and rolling contact fatigue damage resistance under rolling contact conditions. We have conducted these investigations using a two-disk testing machine that accurately reproduces the contact region between the rail and the wheel of an overseas freight railway. We also investigated the hardness and plastic flow of the rolling contact surface and discussed wear governing factors and fatigue damage occurrence mechanisms from tribology and fracture mechanics approaches.

2. Wear and Rolling Contact Fatigue Damage Simulation Tests

2.1 Testing machine

Figure 2 shows the appearance and schematic outline of a two-disk testing machine. Motors drive the wheel disk and the rail disk through belts. Hydraulic systems can also load these disks vertically and horizontally. The wheel axis can be tilted at a certain angle to the rail axis, i.e., at an attack angle.

Table 1 Chemical composition, initial hardness and microstructure of test specimens

Specimen		Carbon content (mass%)	Alloy	Hardness (HV10)	Microstructure
Rail	0.8 mass%C	0.80–0.81	Si,Mn,Cr,V add.	400	Pearlite
				440	
	0.9 mass%C	0.90–0.91		415	
				440	
	1.0 mass%C	1.00		420	
Wheel		0.70		390	

Table 2 Testing conditions

Loading (kN)	Radial: 17.7 Thrust: 11.8
Angle of attack (°)	0.5
Initial contact pressure (MPa)	2 000 (G.C. portion)
The total number of rolling contact cycles	550×10^3
Lubrication and its duration of cycles	Dry (Non-lubrication) / 0×10^3 to 20×10^3 Water (5 cc/min) / 20×10^3 to 320×10^3 Repeated dry (0.5 min) and water (1.0 min) / 320×10^3 to 550×10^3

2.2 Specimens

The chemical composition, initial hardness, and microstructure of the specimens are shown in **Table 1**. The rail specimens were made of steels with carbon contents of 0.8, 0.9, and 1.0 mass% and alloyed with Si, Mn, Cr, and V. (These steels are hereinafter referred to as 0.8, 0.9., and 1.0 mass% C steels.) The wheel specimens were made of steel with a carbon content of 0.7 mass% and alloyed with Si, Mn, Cr, and V.

The steels for the rail and wheel specimens were made by vacuum melting electrolytic iron and ferroalloys. After adjusting the composition by vacuum melting, steel ingots were produced. The ingots were then reheated at 1 250°C and forged to diameters of 220 to 240 mm.

To change the initial hardness of the pearlite structure and prevent the formation of proeutectoid cementite structure, we roughly machined the rail specimens from the forged ingots to a size equivalent to that of the specimens, reheated to a temperature range of 950 to 1 050°C by high-frequency heating, and then acceleratedly cooled at the specified rate. The hardness of the respective test steels was controlled in a range of 400 to 440 HV. On the other hand, the wheel specimens were roughly machined from the forged ingots to a size equivalent to that of the specimens, reheated to 950°C by high-frequency heating, and then acceleratedly cooled. The hardness was adjusted to 390 HV.

The heat-treated rail and wheel specimens were finally machined to a rail cross-sectional shape (AREMA standard 136RE) scaled down to one quarter and to a wheel cross-sectional shape (AAR standard) scaled down to one quarter used for freight railways. The diameter at the middle of the width is 200 mm for both the rail and wheel disk specimens.

2.3 Test conditions

Table 2 shows the test conditions. A motor drove the wheel specimen. The rail specimen was set to rotate freely and was driven by the wheel specimen. To reproduce the contact conditions in a curved section (radius of curvature of 200 to 300 m) of a freight railway with a wheel load of 20 tons, we set the loading conditions at a radial load of 17.7 kN and a thrust load of 11.8 kN. In addition, the angle of attack of the wheel specimen was set to 0.5°. **Figure 3** shows the finite element method (FEM) calculation results of initial contact between the rail and wheel specimens. The rail specimen mainly contacted the wheel specimen in two regions: the head top and gauge corner. The maximum contact pressure p_n in the gauge corner was about 2 000 MPa. The gauge corner comes into contact with the wheel flange throat portion. The rotation radius of the wheel throat portion is larger than that of the gauge corner. Therefore, a tangential force (friction force) acts on the gauge corner in the same direction as the rolling direction (opposite to the direction of load movement).[14]

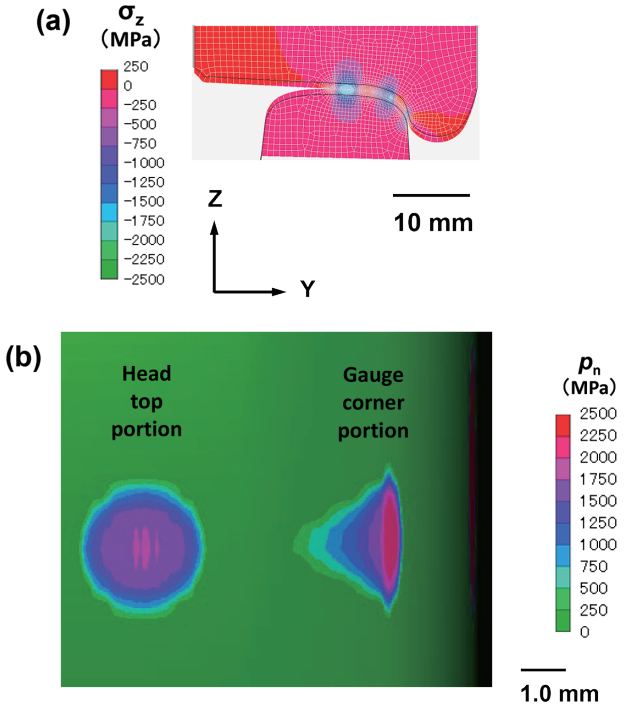

Fig. 3 Pressure and stress distributions of the rail specimen in contact with the wheel specimen under the initial condition: (a) Distribution of vertical stress σ_z, (b) Distribution of normal contact pressure p_n on a rail specimen surface

The number of rolling contact cycles was set to 550×10^3. The lubrication conditions were as follows: the initial 20×10^3 cycles were dry, the next 20×10^3 to 320×10^3 cycles were water lubricated, and the final 320×10^3 to 550×10^3 were alternately dry for 0.5 min and water lubricated for 1.0 min (hereafter referred to as repeated dry and water lubricated cycles). In the water lubricated cycles, water was dripped onto the contact surfaces of both rail and wheel specimens at a rate of 5 cc/min. The aims of these lubrication conditions are as follows: the initial dry run is a break-in run. However, after the initial dry run, the roughness of the rolling surface increases. Therefore, in the subsequent water lubricated run, the contact surface is smoothed like that of an actual rail. At the same time, micro-cracks are generated on the rolling contact surface. In addition,

in the case of repeated dry and water lubricated cycles, in order to reproduce rolling contact fatigue damage resulting from plastic flow, a strong tangential force that develops plastic flow is applied to the rolling contact surface during the dry run. In the subsequent water lubricated run, water penetrates into the inside of the cracks to accelerate their propagation.[15, 16]

2.4 Evaluation

The test was conducted four times for each hardness of the test specimens. After the test, the cross-sectional shape of the rail specimens was measured using a three-dimensional measuring machine with a contact probe to evaluate the wear characteristics. Next, the side opposite the gauge corner and where no wear had occurred was used as the reference, the shape after the test and the initial shape were superimposed on each other, and the difference of the cross-sectional area between the pre- and post-test regions was taken as the amount of wear. In addition, the appearance of the rolling contact surface was observed. The formation of cracks beneath the rolling contact surface and the changes in microstructure and hardness were also investigated. The gauge corner where cracks had been locally generated was cut in the rolling direction, polished, and etched with nital. Then, the microstructure was observed with an optical microscope. In addition, the cross-sectional hardness in the depth direction and beneath the rolling contact surface was measured with a micro Vickers hardness tester (25 gf). The measurement of the cross-sectional shape and the appearance observation of the rolling contact surface were conducted on one cross section of a quarter circumference or on a quarter circumference for each test specimen. Also, for each test specimen, a region with an arc length of 8 mm was selected from the rolling contact surface over a quarter circumference, and the microstructural observation and hardness measurements were conducted in two fields of view within that region.

3. Test Results

3.1 Effects of initial hardness and carbon content on wear resistance

3.1.1 Comparison of wear amount

Figure 4 shows the relationship between the initial hardness and wear amount of rail specimens. Notably, the wear amount decreases as the initial hardness increases, irrespective of the carbon content. A strong correlation is also observed between the wear amount and the carbon content, with the wear amount decreasing significantly as the carbon content increases. When comparing the wear amount of the specimens, the 1.0 mass% C steel (420 HV) is conspicuous with its small wear amount, demonstrating excellent wear resistance.

3.2 Effects of initial hardness and carbon content on rolling contact fatigue damage resistance

3.2.1 Properties of rolling contact surfaces

Figure 5 shows the rolling contact surfaces of typical rail specimens after the test. Small pits and spalls of various sizes are formed and distributed in the gauge corner region along the rolling direction. The length of the largest spalls reaches about 10 mm in the rolling direction. The number and size of spalls vary greatly depend-

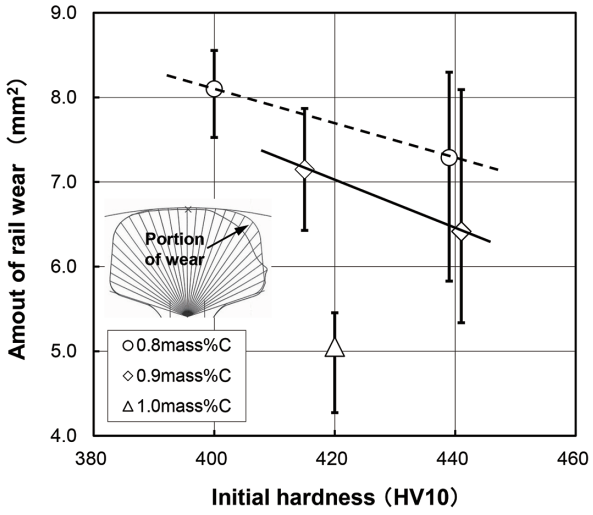

Fig. 4 Relationship between the initial hardness and wear amount of the rail specimens

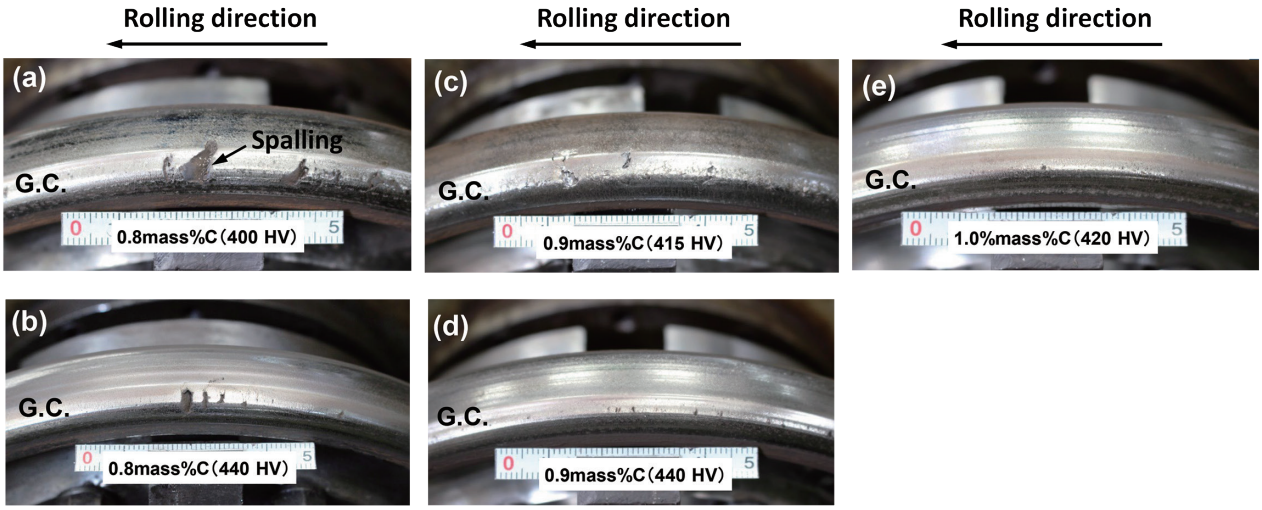

Fig. 5 Typical rolling contact surfaces of the rail specimens after the test:
(a) 0.8 mass%C 400 HV10, (b) 0.8 mass%C 440 HV10, (c) 0.9 mass%C 415 HV10, (d) 0.9 mass%C 440 HV10, (e) 1.0 mass%C 420 HV10

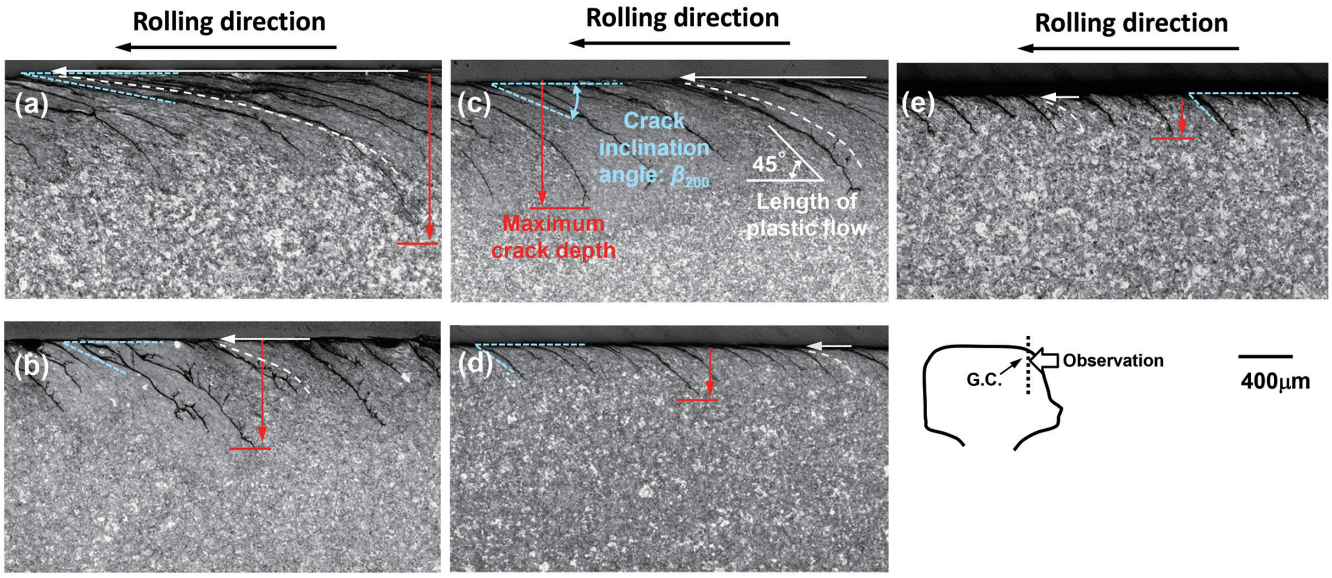

Fig. 6 Typical cross-sectional microstructure beneath the G.C. portion of the rail specimens after the test: (a) 0.8 mass%C 400 HV10, (b) 0.8 mass%C 440 HV10, (c) 0.9 mass%C 415 HV10, (d) 0.9 mass%C 440 HV10, (e) 1.0 mass%C 420 HV10

ing on the initial hardness and carbon content of the specimen. There is a tendency for the number and size of spalls to decrease as the initial hardness of the specimen increases. There also is a tendency for the number and size of spalls to decrease as the carbon content of the specimen increases.

3.2.2 Cross-sectional microstructure beneath rolling contact surface

Figure 6 shows the typical cross-sectional microstructures beneath the rolling contact surface in the gauge corner portion of the rail specimens after the test. In all the specimens, the microstructure beneath the rolling contact surface flows in the rolling direction. In other words, plastic flow is observed near the rolling surface. Many cracks initiate and propagate along this plastic flow. Furthermore, some cracks branch and propagate in the direction of the rolling contact surface.

A detailed comparison of the correlation of the initial hardness and carbon content with the plastic flow and cracks reveals significant findings. The plastic flow decreases notably as the initial hardness of the test specimens increases, regardless of the carbon content. Furthermore, the plastic flow tends to decrease with the increase in the carbon content of the specimens. The propagation of cracks corresponds to the change in the plastic flow, with the crack depth tending to decrease with the increase in the initial hardness and carbon content of the specimens.

3.2.3 Behavior of plastic flow beneath rolling contact surface

Figure 7 shows the relationship between the initial hardness of the rail specimens and the length of plastic flow formed beneath the rolling contact surface in the gauge corner portion after the test. The plastic flow length was evaluated according to the method of Eadie et al.[17] The point where the gradient of the plastic flow reaches 45° was defined as the start point of the plastic flow and the point where the plastic flow reaches the rolling contact surface was defined as the end point, as shown in Fig. 6. The plastic flow length was evaluated along the rolling direction by the distance between these points. Regardless of the carbon content of the specimens, a strong correlation was observed between the plastic flow length and the initial hardness of the specimens. The plastic flow length decreases significantly as the initial hardness increases. Furthermore, the plastic flow length tends to decrease with the increase in the carbon content of the specimens. When the plastic flow length of the specimens is compared, the plastic flow length is short for the 0.9 mass% C steel (440 HV) with high hardness and the 1.0 mass% C steel (420 HV) with high carbon content.

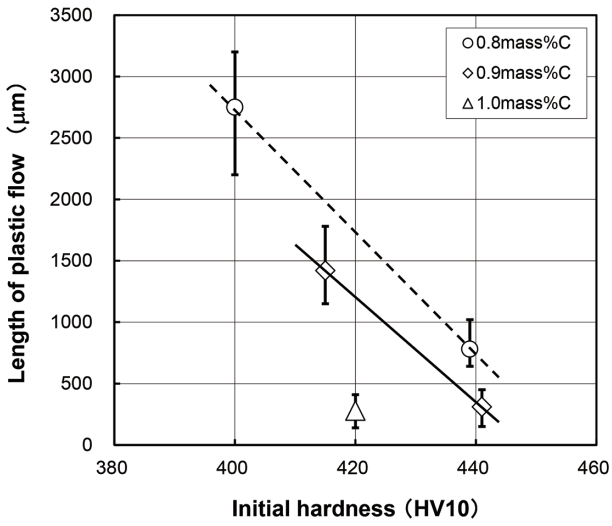

Fig. 7 Relationship between the initial hardness and length of plastic flow formed beneath the G.C. portion of the rail specimens

3.2.4 Behavior of crack angle beneath rolling contact surface

Figure 8 shows the relationship between the initial hardness of the rail specimens and the inclination angle of the crack beneath the rolling contact surface in the gauge corner portion after the test. To quantify the crack formation, we evaluated the inclination angle of

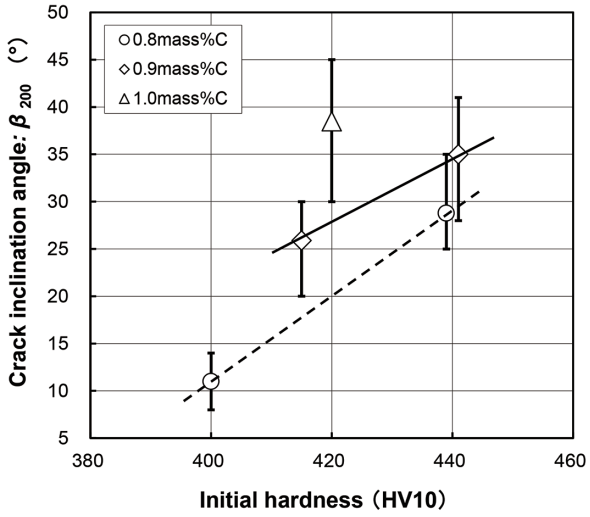

Fig. 8 Relationship between the initial hardness and crack inclination angle beneath the G.C. portion of the rail specimens

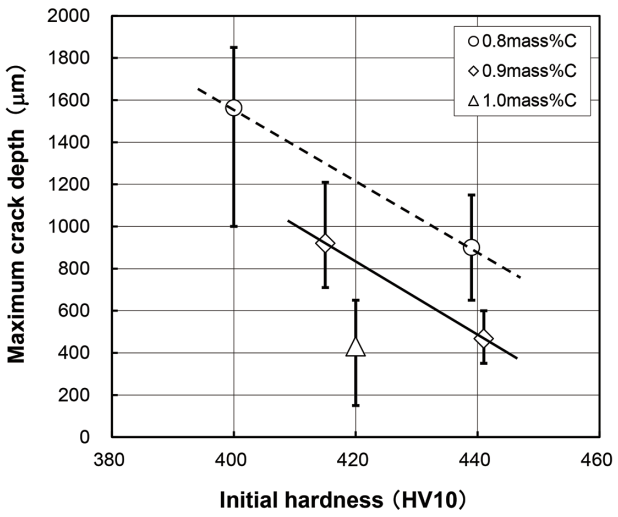

Fig. 9 Relationship between the initial hardness and maximum crack depth beneath the G.C. portion of the rail specimens

the crack formed on the cross section beneath the rolling contact surface in the gauge corner region. The crack inclination angle was defined as the angle (β_{200}) between the line connecting the crack opening and the point at the crack depth of 200 μm and the rolling contact surface, as shown in Fig. 6. Regardless of the carbon content of the specimens, the crack inclination angle was found to be strongly correlated with the initial hardness of the specimens. The crack inclination angle increases significantly as the initial hardness increases. Moreover, the crack inclination tends to increase as the carbon content of the specimens increases. When the specimens are compared by the crack inclination angle, the crack inclination angle is large for the 0.9 mass% C steel (440 HV) with high hardness and the 1.0 mass% C steel (420 HV) with high carbon content.

3.2.5 Crack propagation behavior beneath rolling contact surface

Figure 9 shows the relationship between the initial hardness of the rail specimens and the maximum crack depth beneath the rolling contact surface in the gauge corner portion after the test. For the maximum crack depth, the deepest cracks were measured in a field of view with an arc length of 8.0 mm, as shown in Fig. 6. Regardless of the carbon content of the specimens, a strong correlation was observed between the maximum crack depth and the initial hardness of the specimens. The maximum crack depth decreased significantly as the initial hardness increased. Furthermore, the maximum crack depth shows a tendency to decrease as the carbon content of the specimens increases. When the maximum crack depth of the specimens is compared, the maximum crack depth is small for the high-hardness 0.9 mass% C steel (440 HV) and the high-carbon 1.0 mass% C steel (420 HV). When the surface condition of the rolling contact surface shown in Fig. 6 is also evaluated, these two steels are considered to have excellent resistance to rolling contact fatigue damage.

3.2.6 Change in cross-sectional hardness beneath rolling contact surface

Figure 10 shows the measurement results of cross-sectional hardness distribution beneath the rolling contact surface in the gauge corner portion of the rail specimens after the test. The hardness is shown as the average value measured within a field of view with an arc length of 8.0 mm. Irrespective of the initial hardness or carbon content of the specimens, the hardness near the rolling contact surface increased significantly, and the region where the increase in hardness was observed expanded in the depth direction. A detailed comparison of the correlation between the initial hardness and carbon content of the specimens and the hardness near the rolling contact surface shows that specimens with a high carbon content and high initial hardness tend to have high hardness near the rolling contact surface. When the specimens are compared in the hardness near the rolling contact surface (5 to 10 μm beneath the rolling contact surface), the 1.0 mass% C steel (420 HV) with a high carbon content has the highest hardness.

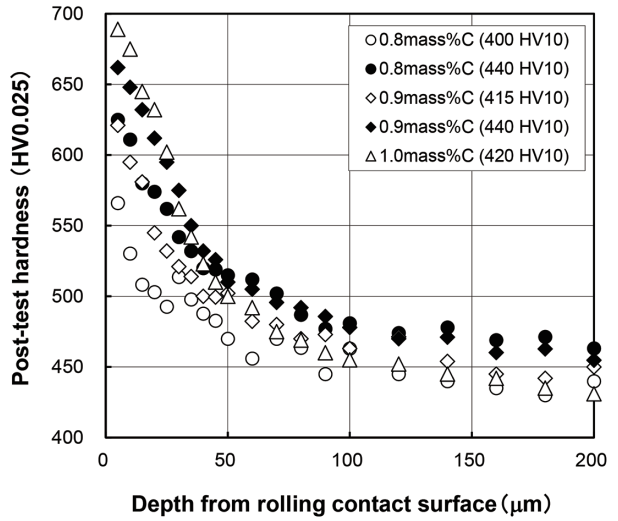

Fig. 10 Hardness distribution beneath the G.C. portion of the rail specimens

4. Mechanisms of Improvement in Wear Resistance and Rolling Contact Fatigue Damage Resistance of High-hardness Pearlitic Steel

As shown in Fig. 4, the wear amount was confirmed to correlate with the initial hardness and carbon content of the rail specimens. It was also confirmed that as the initial hardness and the carbon content of the specimens increase, the wear amount decreases, and the wear resistance improves. Moreover, as shown in Figs. 5, 6, and 9, the rolling contact fatigue damage is correlated with the initial hardness and carbon content of the rail specimens. It was also confirmed that as the initial hardness and carbon content of the specimens increased, the spalling of the rolling surface and the depth of cracks beneath the rolling contact surface decreased, and the rolling contact fatigue damage resistance improved.

In this chapter, we discuss the factors that greatly improved the wear resistance and rolling contact fatigue damage resistance of the specimens by increasing the hardness and carbon content of the pearlitic steel by focusing on the hardness of the rolling contact surface, the development of plastic flow beneath the rolling contact surface, and the changes in the angle and depth of the cracks.

4.1 Mechanism of improvement in wear resistance

Rail wear occurs from rolling contact with the wheel involving slip. The mechanism is considered to be adhesive wear based on the micro shear fracture caused by the plastic deformation of the rolling contact surface.[18, 19] Therefore, the wear of pearlitic steel is confirmed to be closely correlated with the hardness of the rolling contact surface.[6, 20] The test results were thus summarized concerning the relationship between the hardness of the rolling contact surface and wear amount. **Figure 11** shows the relationship between the hardness of the rolling contact surface after the test and the wear amount of the rail specimens. The measurement results shown in Fig. 4 were used to determine the wear amount, and the measurement results of the cross-sectional hardness of the rolling contact surface shown in Fig. 10 were used to determine the hardness of rolling contact surface hardness after the test. The hardness of the rolling contact surface after the test was taken as the average hardness at 5 to 10 μm beneath the rolling contact surface, which is considered to be closest to the rolling contact surface. Regardless of the initial hardness and carbon content of the specimens, the hardness of the rolling contact surface and wear amount are correlated with each other. The wear amount has a confirmed tendency to decrease as the hardness of the rolling contact surface increases. When we also focus on the correlation between the initial hardness and carbon content of the specimens and the hardness of the rolling contact surface after the test, we see that the specimens with high initial hardness and high carbon content show a tendency for the hardness of the rolling contact surface to increase.

Next, to clarify the effect of the initial hardness and carbon content on the hardness increase of the rolling contact surface, we organized the change in the hardness increase rate of the rolling contact surface. **Figure 12** shows the relationship between the initial hardness of the rail specimens and the hardness increase rate of the rolling contact surface. The hardness increase rate (*HIR*) is defined by:

$$HIR(\%) = (PH - IH)/IH \times 100 \quad (1)$$

where *PH* (post-test hardness) is the hardness of the rolling contact surface after the test, and *IH* (initial hardness) is the initial hardness of the rail specimen.

A detailed comparison of the correlation between the hardness increase rate of the rolling contact surface and the initial hardness

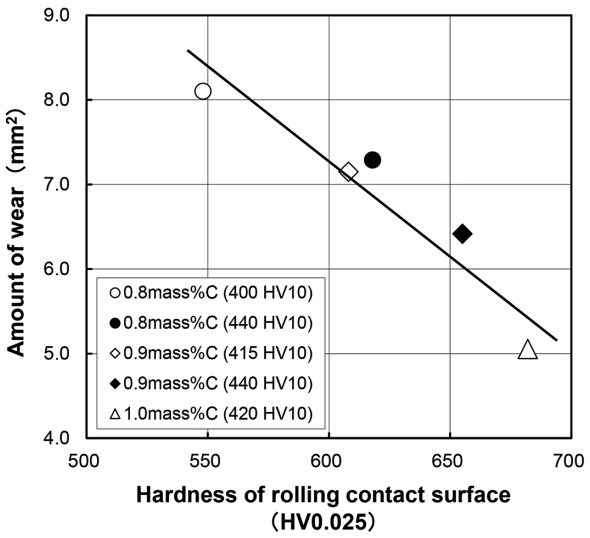

Fig. 11 Relationship between hardness of the rolling contact surface after the test and wear amount of the rail specimens

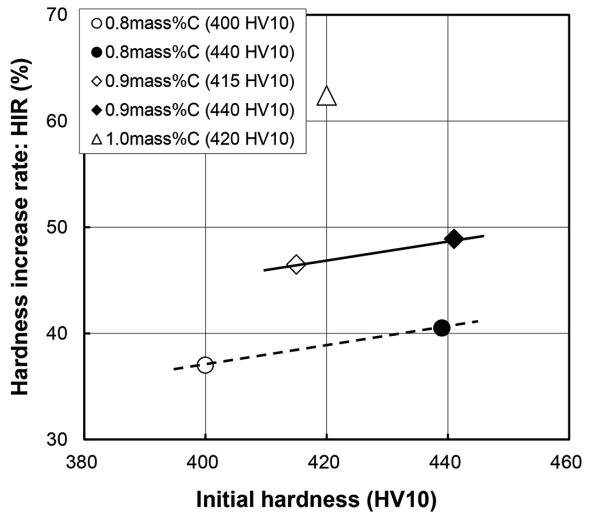

Fig. 12 Relationship between initial hardness and hardness increase rate of beneath the rolling contact surface of the rail specimens

and carbon content of the specimens shows that the effect of the initial hardness on the hardness increase rate of the rolling contact surface is small. In contrast, the effect of the carbon content is extremely large. At the same initial hardness, the hardness increase rate of the rolling contact surface tends to improve significantly as the carbon content increases. The 1.0 mass% C steel (420 HV) with a high carbon content has the largest hardness increase rate of the rolling contact surface.

These results show that the initial hardness of the pearlitic steel is high and that as the carbon content increases, the hardness increase rate improves to increase the hardness of the rolling contact surface. It is then presumed that the wear amount decreases and that the wear resistance of the pearlitic steel improves.

The volume fraction of the cementite phase in the pearlite structure is considered to affect the mechanism by which the hardness in-

crease rate (work hardening rate) of the rolling contact surface increases as the carbon content of the specimens increases. The wear test of the pearlitic steel shows that as the carbon content of the steel or the volume fraction of the cementite phase in the pearlite structure increases, the number of dislocations introduced into the matrix ferrite phase increases and promotes the refinement of the matrix structure. At the same time, the decomposition of the cementite phase is confirmed to promote the solid solution of carbon into the ferrite phase and improve the hardness increase rate.[20] In this test, a similar strengthening mechanism is presumed to have improved the hardness increase rate (work hardening rate) of the rolling contact surface and consequently increased the hardness of the rolling contact surface.

4.2 Mechanism of improvement in rolling contact fatigue damage resistance

Cracks formed in the rolling contact surface of the pearlitic steel initiate from the plastic flow regions and propagate along the plastic flow.[21] Therefore, the development of plastic flow is believed to correlate with the formation and propagation of cracks. In this section, to clarify the effects of the initial hardness and carbon content on the rolling contact fatigue damage property, we discuss the relationship between the initial hardness and carbon content of the rail specimens and the development of the plastic flow beneath the rolling contact surface on the basis of the contact mechanics and the relationship between the development of plastic flow and the crack propagation on the basis of the fracture mechanics.

4.2.1 Effect of initial hardness and carbon content on plastic flow beneath rolling contact surface

The plastic flow at the rolling contact surface is considered to be greatly affected by the tangential force acting on the rolling contact surface. It is organized as a shakedown map, which is calculated and classified based on the relationship between the tangential force coefficient, Hertzian maximum contact pressure, and shear yield strength of steel (k).[22] Under rolling-sliding contact conditions exceeding the shakedown limit, the plastic flow is considered to develop beneath the rolling contact surface and cause damage such as spalling. Therefore, under conditions where the tangential force coefficient and the maximum contact pressure are constant, the shear yield strength of steel (k) has a significant effect on the plastic flow behavior. Generally, when the shear yield strength (k) increases, the shakedown limit is considered to increase and suppress the plastic flow.[23] In this section, we consider the development of the plastic flow beneath the rolling contact surface from the perspective of the hardness beneath the rolling contact surface of the rail specimens, i.e., the shear yield strength.

The post-test shear yield strength (k) beneath the rolling contact surface was estimated from the hardness (HV) beneath the rolling contact surface, tensile strength (σTS), and yield strength (σYP) shown below. First, using the post-test hardness (HV) beneath the rolling contact surface, the tensile strength (σTS) was estimated by the following Eq. (2). Note that the post-test hardness beneath the rolling contact surface was the average hardness value at 5 to 50 μm beneath the rolling contact surface where the microstructure is considered to be most susceptible to the effect of contact. The measurement results of the cross-sectional hardness of the rolling contact surface shown in Fig. 10 were used in this consideration.

$$\sigma TS = 9.8 \times HV/3 \quad (2)$$

where the unit of σTS is MPa. The yield strength (σYP) was estimated from the following Eq. (3). A is the yield ratio. The yield ratio (A) was set to 0.90 according to the tensile test results of cold-worked pearlitic steels.[24]

$$\sigma YP = A \times \sigma TS \quad (3)$$

Furthermore, the shear yield strength (k) beneath the rolling contact surface was estimated from the yield strength (σYP) by using the Mises maximum shear strain energy condition expressed by the following Eq. (4):

$$k = \sigma YP/\sqrt{3} \quad (4)$$

Table 3 shows the estimated results of the shear yield strength (k). Like the hardness of the rolling contact surface shown in Fig. 10, specimens with high initial hardness and high carbon content tend to have high shear yield strength (k). **Figure 13** shows the relationship between the post-test shear yield strength (k) beneath the rolling contact surface and the average plastic flow length. The average plastic flow length was taken as the average value of the plastic flow lengths shown in Fig. 7. Regardless of the initial hardness or carbon content of the specimens, there is a correlation between the post-test shear yield strength beneath the rolling contact surface and the average plastic flow length. The average plastic flow length is recognized as tending to decrease as the post-test shear yield strength increases.

From these results, it is presumed that the hardness beneath the rolling contact surface, i.e., the shear yield strength, increases as the initial hardness and carbon content of the rail specimens increase

Table 3 Estimated results of shear yield strength based on the hardness beneath the rolling contact surface after the test

Specimen	Hardness (HV0.025)	*TS* (MPa)	*YP* (MPa)	*k* (MPa)
0.8 mass%C (400 HV10)	505	1 650	1 485	857
0.8 mass%C (440 HV10)	558	1 823	1 641	947
0.9 mass%C (415 HV10)	541	1 767	1 591	918
0.9 mass%C (440 HV10)	584	1 908	1 717	991
1.0 mass%C (420 HV10)	588	1 921	1 729	998

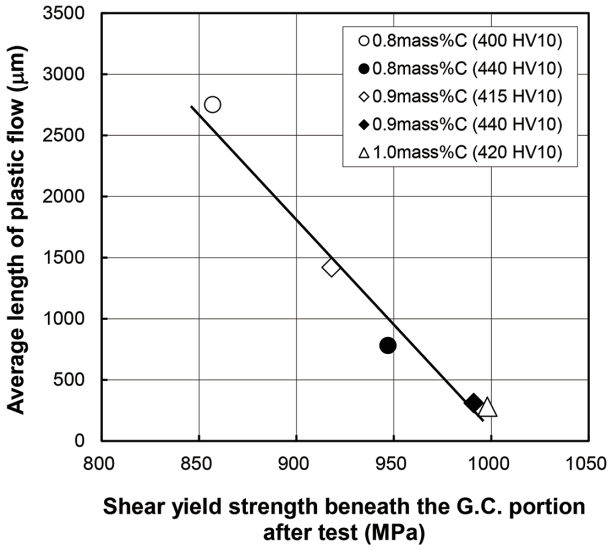

Fig. 13 Relationship between shear yield strength beneath the rolling contact surface after the test and average length of plastic flow

and that the development of the plastic flow on the rolling contact surface is suppressed as the shakedown limit increases.

4.2.2 Effects of initial hardness and carbon content on crack propagation beneath rolling contact surface

The crack propagation mechanism in lubricated rolling-sliding contact has been discussed by many researchers from a fracture mechanics approach (e.g., Keer et al.,[25] Kaneta et al.,[26,27] Bower et al.,[28] Akama et al.[29]). They showed that the water pressure due to fluid penetration into cracks plays an important role in changing the stress intensity factor that determines the stress concentration near the crack tip. Furthermore, Tyfour et al.[15] and Kaneta et al.[16] showed from the results of experiments with two-disk testing machines that the water-lubricated condition after the dry condition or frequent repetition of the dry and water-lubricated conditions strongly affects the crack propagation behavior. In this section, in order to clarify the effects of the initial hardness and carbon content on the rolling contact fatigue damage property, we discuss the effects of the initial hardness and carbon content of rail specimens on the crack propagation behavior beneath the rolling contact surface from the standpoint of fracture mechanics mentioned above.

Figure 14 shows a schematic model of a surface crack in lubricated rolling/sliding contact. This model assumes that the Hertzian contact pressure $p(x)$, accompanied by the surface tangential force $q(x)$, moves in the x direction on an elastic half-space containing a crack with the inclination angle (β) to the surface. In this figure, a and c are the contact half-width and the crack length, respectively. In the gauge corner region of the rail specimen, the surface tangential force $q(x)$ acts in the direction opposite to the load movement.

Based on the above model, each parameter is set using the results of this experiment. As shown in the FEM analysis results of Fig. 3, the contact arc length ($2a$) of the wheel and the gauge corner in the rolling direction was about 3.60 mm. The cracks observed in this experiment exhibited various forms, as shown in Fig. 6. When the representative crack length (c) was measured within the depth range of down to 200 μm beneath the rolling surface, it ranged from 0.32 to 1.12 mm (320 to 1 120 μm). Based on this result, the value of c/a, which affects the stress concentration at the crack tip, was calculated to be in the range of 0.18 to 0.62. The crack inclination angle (β) was in the range of 10 to 41°.

The effect of water penetrating the crack on the propagation behavior of the crack modeled in this experiment is evaluated from the analysis results of the stress intensity factor (SIF) based on the fluid entrapment mechanism in the referenced reports. **Table 4** organizes and presents the crack propagation in the modeled experiment described above and the SIF analysis results up to now. The SIF values in the table are the maximum SIF values when the Hertzian contact pressure distribution moves on the surface. The model of Bower et al.[28] reports that when the Hertzian contact pressure acts near the top of the crack opening, both the opening type K_I value and the shear type K_{II} value increase at the crack tip, and especially the K_I value increases significantly. In addition, the model by Akama et al.[29] reports that the K_I value increases significantly as the crack inclination angle (β) decreases. Also, the K_I value is shown to increase significantly when the crack inclination angle (β) decreases to 25° or less. Furthermore, Makino et al. report that the SIF threshold value $K_{I,th}$ is smaller than the SIF threshold value $K_{II,th}$ according to their analysis of the wheel steel that exhibited a pearlite structure.[30] The increase in the opening type K_I value at the crack tip is estimated to accelerate the crack propagation.

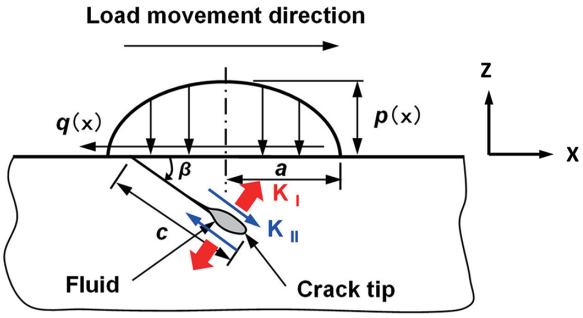

Fig. 14 Schematic model of a surface crack in lubricated rolling/sliding contact

Table 4 Estimated c/a and β in this study and their effects on K_I and K_{II} obtained by Bower and Akama

Results		c/a	β (°)	SIF	
				$K_I/(p_0\sqrt{a})$	$K_{II}/(p_0\sqrt{a})$
Experimentation	0.8 mass%C (400 HV10)	0.62	10	–	–
	0.8 mass%C (440 HV10)	0.30	28	–	–
	0.9 mass%C (415 HV10)	0.36	27	–	–
	0.9 mass%C (440 HV10)	0.21	36	–	–
	1.0 mass%C (420 HV10)	0.18	41	–	–
Bower[28]		0.50	25	0.16	0.14
Akama[29]		0.50	50	0.11	0.18
			25	0.18	0.12
			12.5	0.30	0.07

From these results, we estimate the crack propagation in rail specimens with different initial hardness and carbon content. As shown in Fig. 8 and Table 4, the crack inclination angle is small in specimens with low initial hardness and carbon content. As a result, the K_I value at the crack tip increases significantly due to the water penetration into the crack. The crack tip is estimated to be in the condition where the crack propagation is easily promoted. On the other hand, in specimens with high initial hardness and carbon content, the crack inclination angle is large, and the increase in the K_I value is inhibited compared to specimens with low initial hardness and carbon content. The crack tip is estimated to be in the condition where the crack propagation is not easily promoted.

4.2.3 Spalling mechanism of pearlitic steel

In this section, we consider the mechanism of spalling in pearlitic steel based on our study results. **Figure 15** schematically illustrates the microstructural change beneath the rolling contact surface of the gauge corner portion in the rail specimens, the crack propagation behavior, and the spalling occurrence. As shown in Fig. 6, the initial crack occurs from the plastic flow region and propagates along the plastic flow. In pearlitic steel with low initial hardness and carbon content, the shear yield strength (k) beneath the rolling contact surface is low. On the other hand, in pearlitic steel with high

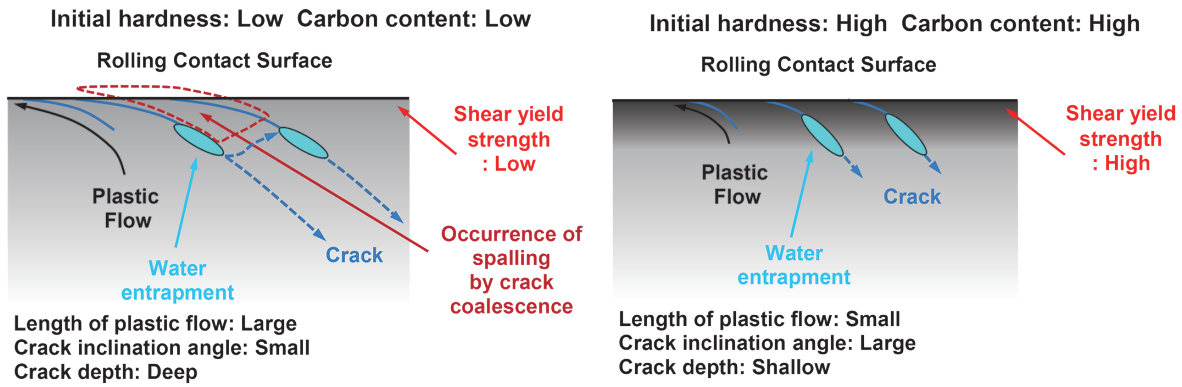

Fig. 15 Schematic illustration of structural variation, behaviour of crack propagation, and occurrence of spalling beneath the G.C. portion of the rail specimens

initial hardness and carbon content, the shear yield strength (k) beneath the rolling contact surface is high. Therefore, in the pearlitic steel with the low shear yield strength (k), the plastic flow is likely to develop, and the inclination angle (β) of the crack that initiated and propagated along the plastic flow is likely to decrease. On the other hand, in the pearlitic steel with high shear yield strength (k), the development of the plastic flow is small, and the inclination angle (β) of the crack that propagated along the plastic flow is considered difficult to decrease. As a result, when water penetrates into a crack under water lubrication, the inclination angle of the crack is smaller in the pearlitic steel with low initial hardness and carbon content than in the pearlitic steel with high initial hardness and carbon content. This situation is considered to increase the K_I value contributing to the opening of the crack tip, promote the crack propagation, and increase the crack depth.

Furthermore, the analysis results of Makino et al.[30] show that the $K\sigma(\theta)$ value (the stress intensity factor in the circumferential direction around the crack tip) reaches its maximum value in the direction toward the rolling contact surface even when the crack is long (c/a=4.0) and the water pressure inside the crack is low. The crack may branch toward the rolling contact surface. Therefore, in the pearlitic steel with low initial hardness and carbon content, the crack propagates deeply and easily branches toward the rolling contact surface. It is possible that the crack coalesced with surrounding cracks and promoted the spalling of the rolling contact surface.

Due to the mechanism described above, the pearlitic steel with high initial hardness and carbon content has higher shear yield strength (k) beneath the rolling contact surface and is less susceptible to plastic flow as compared to the pearlitic steel with low initial hardness and carbon content. This condition suppresses the decrease in the crack inclination angle (β) and the increase in the K_I value at the crack tip. This effect is presumed to inhibit the crack propagation and greatly improve the rolling contact fatigue damage resistance.

5. Conclusions

We evaluated the wear resistance and rolling contact fatigue damage resistance of pearlitic steels with different initial hardness and carbon content (400 to 440 HV and 0.8 to 1.0 mass% C) by using a two-disk testing machine that simulates rolling contact between a rail and a wheel. The following conclusions were obtained:

(1) The wear amount decreases as the initial hardness and carbon content of the pearlitic steels increase.

(2) The wear resistance of the pearlitic steels is strongly correlated with the carbon content. The wear resistance improves greatly as the carbon content increases.

(3) The improvement in the wear resistance of the pearlitic steels with the increase in the carbon content is considered attributable to the increase in the hardness increase rate (work hardening rate) of the rolling contact surface, i.e., the increase in the hardness of the rolling contact surface.

(4) As the initial hardness and carbon content of the pearlitic steels increase, the spalling of the rolling contact surface decreases. Furthermore, the depth of the crack propagating beneath the rolling contact surface decreases, thereby significantly improving the rolling contact fatigue damage resistance.

(5) As the initial hardness and carbon content of the pearlitic steels increase, the shear yield strength beneath the rolling contact surface increases, the development of the plastic flow is suppressed, and the decrease in the inclination angle of the crack beneath the rolling contact surface is inhibited.

(6) A crack with a large inclination angle suppresses the stress concentration at the crack tip due to the penetration of water into the crack. The crack propagation in a pearlitic steel with high initial hardness and carbon content and a large crack inclination angle inhibits the crack propagation compared to a pearlitic steel with low initial hardness and carbon content and a small crack inclination angle. As a result, the rolling contact fatigue damage resistance is considered to improve.

References

1) Wessels, L., Oswald, S., Welsby, D., Mutton, P.: In Proceedings of the International Heavy Haul Conference, Perth, 1045 (2015)
2) Ghonem, H., Kalousek, J., Stone, D.H., Laufer, E.E.: In Proceedings of the 2nd International Heavy Haul Conference, Colorado Springs, 339 (1982)
3) Muster, H., Schmedders, H., Wick, K., Pradier, H.: Wear. 191, 54 (1996)
4) Clayton, P.: Wear. 191, 170 (1996)
5) Magel, E., Mutton, P., Ekberg, A., Kapoor, A.: Wear. 366–367, 249 (2016)
6) Kageyama, H., Sugino, K., Masumoto, H.: Tetsu-to-Hagané. 64 (11), S905 (1978)
7) Ueda, M., Takehara, J., Iwasaki, N., Ichinose, H.: Tetsu-to-Hagané. 64 (11), S906 (1978)
8) Brave, G., Hannafious, J., Steele, R.: AAR Report. R-796, (1991)
9) Ueda, M., Uchino, K., Kobayashi, A.: Wear. 253, 107 (2002)
10) Beynon, J.H., Garnham, J.E., Sawley, K.J.: Wear. 192, 94 (1996)
11) Stock, R., Pippan, R.: Wear. 314, 125 (2011)
12) Stock, R., Pippan, R.: Wear. 314, 44 (2014)
13) Ueda, M., Matsuda, K.: Wear. 444–445, 203120 (2020)

14) Heathcote, H.L.: The Ball Bearing. Proceedings of the Institution of Automobile Engineers. 15, 569 (1920)
15) Tyfour, W.R., Beynon, J.H., Kapoor, A.: Wear. 197, 255 (1996)
16) Kaneta, M., Matsuda, K., Murakami, K., Nishikawa, H.: J. Tribol. 120, 304 (1998)
17) Eadie, D.T., Elvidge, D., Oldknow, K., Stock, R., Pointner, P., Kalousek, J., Klauser, P.: Wear. 265, 1222 (2008)
18) Sasada, T.: J. Jpn. Soc. Lubr. Eng. 24 (11), 700 (1979)
19) Yamamoto, Y., Kaneda, Y.: Tribology. First edition. Tokyo, Rikogakusha, 1998, 190p
20) Ueda, M., Uchino, K., Senuma, T.: Tetsu-to-Hagané. 87 (4), 190 (2001)
21) Sato, M., Anderson, P.M., Rigney, D.A.: Wear. 162–164, 159 (1993)
22) Johnson, K.L.: Contact Mechanics. Cambridge University Press, 1985
23) Jones, C.P., Tyfour, W.R., Beynon, J.H., Kapoor, A.: In Proceedings of the Institution of Mechanical Engineers, 211, 131 (1997)
24) Liu, Y., Yang, C.D., Liu, M., Wang, C.H., Dai, Y.C., Li, X., Russell, A.M., Zhang, C.X., Zhang, H., Cao, G.H.: Materials Science & Engineering. A709, 115 (2018)
25) Keer, L.M., Bryant, M.D.: ASME Journal of Lubrication Technology. 105, 198 (1983)
26) Kaneta, M., Murakami, Y.: Tribology International. 20 (4), 210 (1987)
27) Kaneta, M., Murakami, Y.: ASME Journal of Tribology. 113, 270 (1991)
28) Bower, A. F.: ASME Journal of Tribology. 110, 704 (1988)
29) Akama, M., Mori, T.: Transactions of JSCES. No.20070012 (2007)
30) Makino, T., Kato, T., Hirakawa, K.: International Journal of Fatigue. 36, 68 (2012)

Masaharu UEDA
Dr. Eng., General Manager
Rail & Shape Div.
Kyushu Works
1-1 Tobihata-cho, Tobata-ku, Kitakyushu City,
Fukuoka Pref. 804-8501

Takeshi YAMAMOTO
Chief Manager
Quality Management Div.
Kyushu Works

Kyohei SONOYAMA
Chief Manager
Rail & Shape Quality Control Dept.
Quality Management Div.
Kyushu Works